



CDK4/6i reverse PARPi resistance by targeting the E2F1- MCM2/5 pathway



Yujie Feng^{1,2,8}, Miao Fu^{1,8}, Bowen Zheng^{1,2,3,8}, Fanzhuoran Lou^{2,8}, Xintian Huang², Xiaowen Xie¹, Weijuan Tan², Quan Chen², Wenqing Zhang¹, Yongxiang Hong^{2,4}, Kaiyi Rong², Huibo Shi⁵ ✉, Tianhui Hu^{1,6,7} ✉ & Li Xiao² ✉

Resistance to poly (ADP-ribose) polymerase inhibitors (PARPis) like niraparib represents a major therapeutic challenge in ovarian cancer (OC). This study elucidates a novel resistance mechanism driven by the minichromosome maintenance proteins 2 and 5 (MCM2/5). In niraparib-resistant (NirR) OC cells, RNA-seq revealed upregulation of MCM2 and MCM5, which was functionally linked to enhanced proliferation and homologous recombination repair. Co-immunoprecipitation confirmed strengthened MCM2/5 interaction in NirR cells. Genetic knockdown of MCM2/5 resensitized NirR cells to niraparib, while their overexpression conferred resistance in parental cells. Mechanistically, the upregulation of MCM2/5 was transcriptionally regulated by the E2F1 transcription factor, activated via the CDK4/6-RB pathway. Consequently, pharmacological inhibition of CDK4/6 downregulated MCM2/5 expression and, when combined with niraparib, synergistically suppressed NirR tumor growth both in vitro and in vivo. Our findings identify the MCM2/5 complex as a critical mediator of PARPi resistance and establish the therapeutic potential of combining PARPis with CDK4/6 inhibitors to overcome this resistance in ovarian cancer.

Ovarian cancer (OC) is the deadliest gynecologic malignancy and has a high death-to-incidence ratio globally, with incidences of 313,959 and deaths of 207,252 per year^{1,2}. OC, especially high-grade serous ovarian cancer (HGSOC), is mostly diagnosed at an advanced stage and responds to first-line treatment with cytoreductive surgery and platinum-based chemotherapy. However, approximately 85% of OC patients will relapse following initial surgery and chemotherapy within two years and eventually die of OC³. This highlights a significant and urgent need to develop new therapeutic strategies to overcome acquired resistance to systemic therapy.

PARPi exploits inherent defects in homologous recombination repair (HRR) capacity and leads to synthetic lethality^{4,5}. Several PARPis, olaparib, rucaparib, niraparib, and fluzoparib, have consequently become standard targeted treatments for OC⁵. However, inherent or acquired resistance to PARPi is inevitable. Previous studies have shown that resistance to PARPis mostly occurs via three general mechanisms, including restoration of HRR,

mitigation of replication stress, and upregulation of drug efflux pumps⁶. A deeper understanding of the molecular drivers of resistance is urgently needed to identify novel mechanisms and develop rational strategies, such as combination therapies or post-progression interventions, to overcome this challenge.

During the cell cycle, minichromosome maintenance proteins (MCMs) are essential for DNA replication initiation and extension, which is vital for maintaining genomic integrity. Dysregulation of DNA replication contributes to the initiation and progression of cancer. MCMs are reported to be essential to tightly regulate DNA replication for maintaining normal cellular processes, especially in the DNA initiation and elongation stages. Aberrant expression or activity of MCMs is frequently detected in various cancers, including gastrointestinal cancers, lung, brain, renal, breast, ovarian, and blood cancers, etc.^{7–12}. MCMs play an important role in the occurrence and development of cancers and may be an important target for

¹Xiamen Key Laboratory for Tumor Metastasis, Cancer Research Center, School of Medicine, Xiamen University, Xiamen, China. ²Department of Oncology, Zhongshan Hospital of Xiamen University, School of Medicine, Xiamen University, Xiamen, China. ³National Institute for Data Science in Health and Medicine, Xiamen University, Xiamen, China. ⁴The Graduate School of Fujian Medical University, Fujian Medical University, Fuzhou, 350122 Fujian, China. ⁵Institute of Organ Transplantation, Tongji Hospital, Tongji Medical College, Huazhong University of Science and Technology, Wuhan, China. ⁶Shenzhen Research Institute of Xiamen University, Shenzhen, China. ⁷Key Laboratory of Prevention and Treatment of Cardiovascular and Cerebrovascular Diseases (Ministry of Education), Gannan Medical University, Ganzhou, China. ⁸These authors contributed equally: Yujie Feng, Miao Fu, Bowen Zheng, Fanzhuoran Lou. ✉e-mail: jimshihuibo@163.com; thu@xmu.edu.cn; xlshb0826@xmu.edu.cn

cancer diagnosis and treatment. Nine members (MCM2, MCM3, MCM4, MCM5, MCM6, MCM7, MCM8, MCM9, and MCM10) of the MCM family have been identified in humans, and each member has distinct functions in DNA replication⁹. The MCM2–7 complex functions as both an AAA+ ATPase and a DNA replicative helicase, contributing to the formation of the pre-replicative complex and is required for DNA replication¹³.

Building on previous work on PARPi resistance mechanisms, we focused on investigating the role of MCM2 and MCM5 in the development of niraparib resistance (NirR) in ovarian cancer cells. In this report, RNA-Seq results suggested that the MCM family genes were downregulated after niraparib treatment in OC cells. However, in NirR OC cells, MCMs were significantly upregulated, which suggested that MCMs were closely related to niraparib resistance. Additionally, database analysis revealed that increased mRNA expression of MCM2/5 correlated with poor overall survival (OS) in OC patients, further suggesting their role in promoting resistance. Upregulated MCM2/5 mediated PARPi resistance, and MCM2/5 downregulation rescued the sensitivity to PARPi in OC cells. MCM2/5 downregulation inhibited proliferation and reduced the proportion of cells in S-phase in NirR OC cells. In resistant cells, the upregulation of MCM2/5—along with their enhanced interaction—conferred this resistance by inducing concomitant upregulation of HRR genes and reducing DNA damage. RNA-Seq results showed that *CDK4/6* were significantly upregulated along with *MCM2/5* in NirR cell lines. Based on this finding, we studied the combination treatment of *CDK4/6* inhibitor (dalpiciclib) and PARPi (niraparib) in NirR OC and found that the combination treatment could reverse niraparib resistance and downregulate MCM2/5.

Results

Development and Identification of Niraparib-Resistant Ovarian Cancer Cell Lines

Following the previously reported method, we successfully established niraparib-resistant (NirR) cell lines (A2780R and SKOV3R). Figure 1A illustrates the workflow for establishing niraparib-resistant ovarian cancer cells. The IC₅₀ value of niraparib in parental A2780 cells was $16.22 \pm 0.98 \mu\text{M}$, and in parental SKOV3 cells was $74.13 \pm 2.32 \mu\text{M}$. In contrast, the IC₅₀ values in A2780R and SKOV3R cells increased to $63.10 \pm 1.26 \mu\text{M}$ and $173.78 \pm 4.34 \mu\text{M}$, respectively, corresponding to resistance indices of 5.65 and 3.78 (Fig. 1B). Consistent with this, niraparib treatment profoundly inhibited the proliferation of parental A2780 and SKOV3 cells, but had minimal effects on NirR cells (A2780R and SKOV3R) (Fig. 1C, D). Similarly, niraparib treatment significantly reduced clonogenic survival of A2780 and SKOV3 cells, while having minimal effects on the NirR cells (Fig. 1E, F). The EdU assay revealed that Niraparib significantly inhibited the proliferation of A2780 and SKOV3 cells, whereas it had minimal effect on the proliferation of A2780R and SKOV3R cells (Fig. 1G, H). Figure 1, I, J demonstrates that the cell cycle of A2780 and SKOV3 cell lines was arrested at the G₂/M phase by Niraparib, whereas the cell cycles of A2780R and SKOV3R cell lines were unaffected. These results confirm the successful establishment of niraparib-resistant cell lines, setting the stage for further exploration of the mechanisms underlying drug resistance.

Transcriptomic Profiling Identifies MCM2/5 as Key Mediators of PARP Inhibitor Resistance

To investigate the effects of niraparib on downstream signaling pathways in ovarian cancer cells and explore the mechanisms of PARP inhibitor resistance, we performed RNA-sequencing (RNA-Seq) on parental A2780 cells treated with niraparib and further compared the transcriptomic profiles of A2780 and A2780R cells.

RNA-seq of niraparib-treated A2780 cells identified 9693 differentially expressed protein-coding genes (4643 upregulated and 5053 downregulated; >2-fold) compared to controls, as visualized in the volcano plot (Fig. 2A). Kyoto Encyclopedia of Genes and Genomes (KEGG) pathway enrichment analysis revealed significant changes in 20 pathways (q -value < 0.05) in niraparib-treated A2780 cells (Fig. 2B). Conversely, niraparib-treated A2780R cells exhibited 9186 altered genes relative to

parental cells (4376 up, 4810 down; Fig. 2C), with 20 pathways significantly changed (q -value < 0.05, Fig. 2D). Real-time PCR validation confirmed the RNA-Seq results, showing significant upregulation of *CDKN1A*, *CYFIP2*, *DDB2*, *NID1*, *PHLDA3*, *PLXNB2*, and *XDXR* in niraparib-treated A2780 cells (Supplementary Fig. 1A), while *TUBA1B*, *PHGDH*, *MCM6*, *MKI67*, *ASNS*, *MCM2*, and *MCM5* exhibited significantly reduced mRNA levels (Supplementary Fig. 1B). In niraparib-treated A2780R cells, *PXDNL*, *CDK4*, *CDK6*, *MCM2*, and *MCM5* were significantly upregulated (Supplementary Fig. 1C), whereas *GPM6A*, *ZFHX4*, *PNOX*, *NR4A2*, and *ANK3* mRNA levels were significantly lower compared to parental A2780 cells (Supplementary Fig. 1D). Intersecting the downregulated genes in drug-treated parental cells with the upregulated genes in resistant cells, we identified candidate genes potentially associated with drug sensitivity and resistance, including MCM2, MCM5, and 867 other genes (Supplementary Fig. 2A). Furthermore, analysis via GEPIA indicated that MCM2/5 mRNA expression was significantly higher in ovarian cancer tissues than in normal tissues (Supplementary Fig. 2B). Kaplan-Meier Plotter analysis revealed that elevated MCM2/5 mRNA expression was significantly negatively correlated with progression-free survival (PFS) in ovarian cancer patients (Supplementary Fig. 2C, $P < 0.05$). Supplementary Fig. 2D indicates a positive correlation between MCM2 and MCM5 expression in ovarian cancer tissues ($R = 0.6$, $P < 0.001$). Subsequent experiments showed that PARP inhibitor treatment downregulated MCM2/5 in parental ovarian cancer cell lines (Fig. 2E–G), while MCM2/5 expression was significantly upregulated in niraparib-resistant cells compared to parental sensitive cell lines (Fig. 2H, I). To investigate the interaction between MCM2 and MCM5, we co-transfected 293T cells with FLAG-MCM2 and HA-MCM5 fusion proteins. Co-immunoprecipitation (Co-IP) assays were performed to detect the interaction between MCM2 and MCM5. Immunoblotting results demonstrated that both MCM2 and MCM5 were present in the reciprocal immunoprecipitates, indicating a direct association between MCM2 and MCM5. (Supplementary Fig. 2E). Notably, Niraparib treatment reduced the MCM2-MCM5 interaction in parental cells, while in Niraparib-resistant cells, the interaction was significantly enhanced compared to drug-treated parental cells (Fig. 2J). Based on previous studies, MCM proteins play crucial roles in DNA replication, DNA damage response, and homologous recombination repair^{14,15}. Consistent with these findings, our Western blot analysis demonstrated that the expression of MCM2 and MCM5 remained unchanged following Niraparib treatment in A2780R and SKOV3R cells. Notably, γ -H2AX levels were decreased, while RAD51 expression—an essential gene involved in homologous recombination repair—was increased. These results suggest a potential reduction in DNA damage and enhanced homologous recombination repair (HRR) activity in Niraparib-resistant cells. (Fig. 2K). We also established an A2780 cell line resistant to the PARP inhibitor fluzoparib (Supplementary Fig. 3A). In parental A2780 cells, fluzoparib treatment downregulated MCM2/5 expression (Supplementary Fig. 3B). In contrast, the Fluzoparib-resistant (A2780R) cells exhibited a concomitant upregulation of MCM2/5 and RAD51, alongside a downregulation of γ -H2AX expression (Supplementary Fig. 3C). Consistent with the MCM2/5 upregulation, we observed a more pronounced interaction between MCM2 and MCM5 in these resistant cells (Supplementary Fig. 3D). These findings suggest that high MCM2/5 expression is significantly associated with poor PFS in ovarian cancer patients and that MCM2/5 may mediate acquired PARP inhibitor resistance in ovarian cancer, which is further explored in the following sections.

Functional role of MCM2/5 in Acquired Niraparib Resistance in Ovarian Cancer

Building on the identification of MCM2/5 as potential mediators of PARP inhibitor resistance, we investigated their functional role in ovarian cancer cells. We knocked down MCM2/5 in niraparib-resistant cells and achieved efficient knockdown, as verified by RT-PCR and Western blot (Supplementary Fig. 4A, B). Conversely, we overexpressed MCM2/5 in the parental cell lines, with the successful overexpression confirmed by RT-PCR and Western blot analysis (Supplementary Fig. 4C, D). Cell viability assays

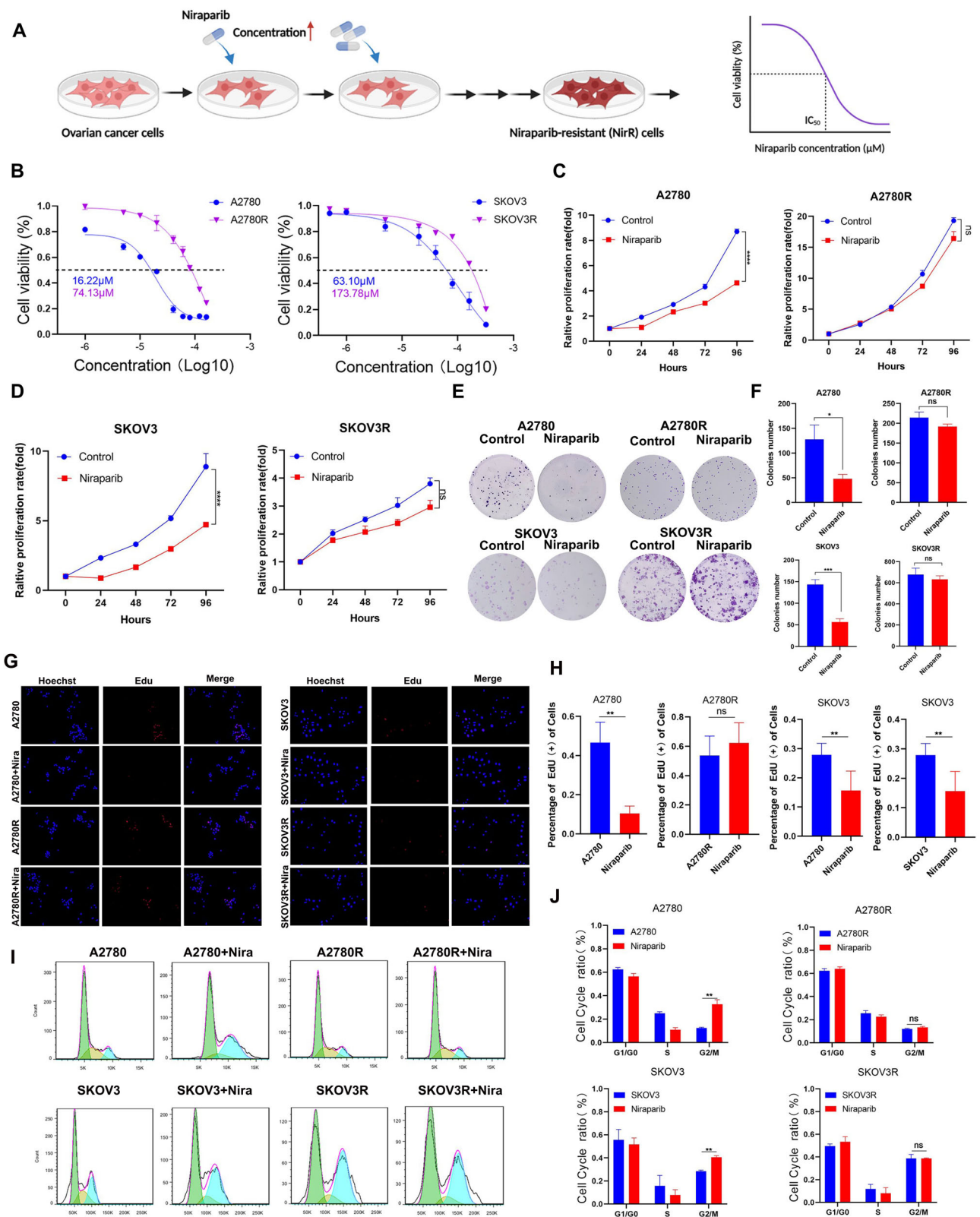
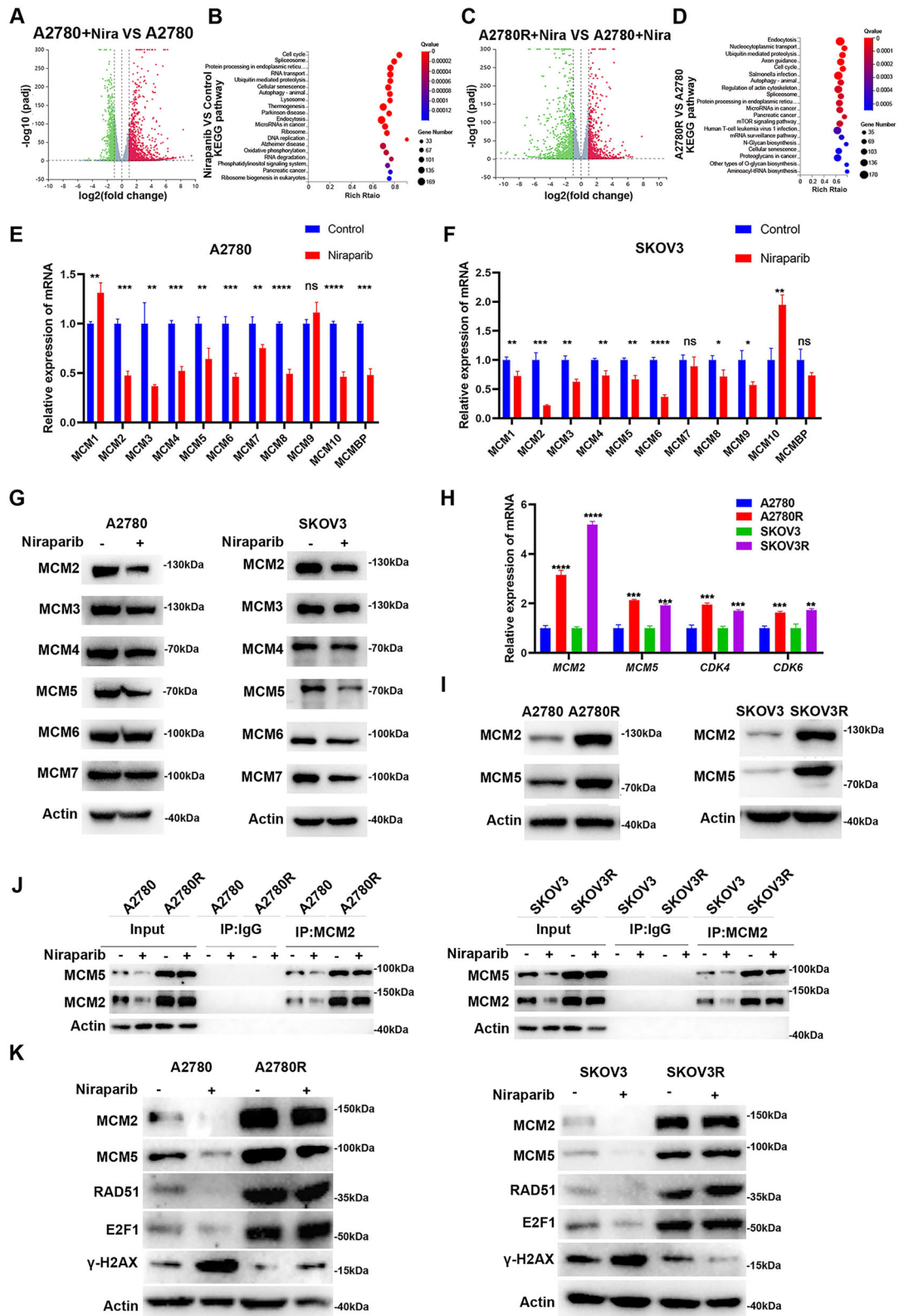


Fig. 1 | Characterization of A2780R and SKOV3R cell lines with acquired niraparib resistance. **A** Construction of niraparib-resistant ovarian cancer cell lines by continuous drug stimulation of ovarian cancer cell lines for 6 months. **B** The IC₅₀ values of niraparib in A2780, A2780R, SKOV3, and SKOV3R cell lines. **C** Proliferation of A2780 and A2780R cells after treatment with niraparib. **D** Proliferation of SKOV3 and SKOV3R cells after treatment with niraparib. **E** Colony formation of A2780 and A2780R cells after treatment with niraparib. **F** Colony formation of SKOV3 and

SKOV3R cells after treatment with niraparib. **G** EdU assay of A2780, A2780R, SKOV3, and SKOV3R cells after treatment with niraparib. **H** EdU formation of A2780, A2780R, SKOV3, and SKOV3R cells after treatment with niraparib. **I** Cell cycle distributions of A2780, A2780R, SKOV3, and SKOV3R following treatment with niraparib. **J** Cell cycle formation of A2780, A2780R, SKOV3 and SKOV3R cells after treatment with niraparib **P* < 0.05, ***P* < 0.01, ****P* < 0.001, *****P* < 0.0001.



revealed that MCM2/5 downregulation could restore sensitivity to niraparib in resistant ovarian cancer cells. The IC₅₀ value of niraparib in A2780R-shctrl MCM2 cells was 50.1 ± 0.96 μM, compared to 24.54 ± 1.03 μM in A2780R-shMCM2-1 cells and 33.84 ± 0.84 μM in A2780R-shMCM2-2 cells. For MCM5, the IC₅₀ value in A2780R-shctrl cells was 50.11 ± 0.93 μM, while it was 25.1 ± 1.02 μM in A2780R-shMCM5-1 cells

and 34.6 ± 1.04 μM in A2780R-shMCM5-2 cells (Fig. 3A). In SKOV3R cells, the IC₅₀ value of niraparib in SKOV3R-shctrl MCM2 cells was 47.86 ± 0.83 μM, compared to 16.59 ± 0.97 μM in SKOV3R-shMCM2-1 cells and 33.88 ± 1.07 μM in SKOV3R-shMCM2-2 cells. For MCM5, the IC₅₀ value in SKOV3R-shctrl cells was 47.86 ± 0.63 μM, while it was 19.95 ± 0.72 μM in SKOV3R-shMCM5-1 cells and 25.11 ± 0.72 μM in

Fig. 2 | Transcriptomic analysis highlighting the upregulation of MCM2 and MCM5 in Niraparib-resistant ovarian cancer cell lines. **A** Volcano plot of the differentially expressed genes in control and niraparib-treated A2780 cells. Red dots represent up-regulated genes and green dots represent down-regulated genes. **B** KEGG pathway enrichment of differentially expressed genes between control and niraparib-treated A2780 cells. **C** Volcano plot of the differentially expressed genes in niraparib-treated A2780 and A2780R cells. Red dots represent up-regulated genes and green dots represent down-regulated genes. **D** KEGG pathway enrichment of differentially expressed genes between niraparib-treated A2780 and A2780R cells. **E** Real-time PCR assays to determine mRNA expression levels of MCMs and MCMBP in A2780 cells after 48 h of niraparib treatment. **F** Real-time PCR assays to

determine mRNA expression levels of MCMs and MCMBP in SKOV3 cells after 48 h of niraparib treatment. **G** Western blots of A2780 and SKOV3 cells of MCM2-7 under niraparib treatment. **H** The mRNA expressions of *MCM2*, *MCM5*, *CDK4*, and *CDK6* were examined by real-time PCR assays between parental and niraparib-resistant cells. **I** The protein expressions of MCM2 and MCM5 were examined by western blot assays between parental and niraparib-resistant cells. **J** Co-IP assay revealing the altered MCM2–MCM5 interaction in A2780, A2780R, SKOV3, and SKOV3R cells following niraparib treatment versus control. **K** The expressions of MCM2, MCM5, RB, P-RB, RAD51, E2F1, and γ H2AX were examined by western blot assays between A2780, A2780R, SKOV3 and SKOV3R. * $P < 0.05$, ** $P < 0.01$, *** $P < 0.001$, **** $P < 0.0001$.

SKOV3R-shMCM5-2 cells (Fig. 3B). Furthermore, we found that MCM2/5 overexpression promoted drug resistance in both A2780 and SKOV3 cells. The resistance indices for A2780 and SKOV3 cells with MCM2 overexpression were 4.17 and 1.91, respectively, and 5.49 and 3.09 for MCM5 overexpression (Supplementary Fig. 5A). These findings confirm that upregulated MCM2/5 contributes to PARP inhibitor resistance, and that MCM2/5 downregulation can resensitize PARPi-resistant ovarian cancer cells to PARP inhibitors. To further investigate the effects of MCM2/5 on cell proliferation, we performed EdU assays. Knockdown of either MCM2 or MCM5 in A2780R or SKOV3R cells significantly suppressed cell proliferation, indicating that MCM2/5 are essential for maintaining DNA replication in these resistant cells (Fig. 3C–F). Moreover, the cell cycle analysis showed that MCM2/5 knockdown led to a significant decrease in the percentage of cells in the S phase, coupled with a concomitant increase in the G1 phase population, suggesting that MCM2/5 downregulation induces G1 phase cell cycle arrest (Fig. 3G, H). Conversely, overexpression of MCM2/5 in A2780 and SKOV3 cells significantly promoted cell proliferation (Supplementary Fig. 5B). Flow cytometric analysis revealed that overexpression of MCM2/5 in these cells resulted in significant cell cycle arrest at the S phase (Supplementary Fig. 5C). We also performed co-immunoprecipitation (Co-IP) assays to investigate the interaction between MCM2 and MCM5. In A2780R and SKOV3R cells, knockdown of MCM2 reduced the amount of MCM5 co-immunoprecipitated, and vice versa, knockdown of MCM5 reduced the co-IP-captured MCM2 (Fig. 3I, J). Additionally, MCM2/5 knockdown in A2780R and SKOV3R cells led to a concomitant increase in the DNA damage marker γ H2AX and decreased RAD51 expression, indicating an impaired DNA damage response (Fig. 3K, L). In contrast, overexpression of MCM2/5 in A2780 and SKOV3 cells promoted the amount of MCM5 captured by co-immunoprecipitation, and correspondingly, overexpression of MCM5 reduced the co-IP-captured MCM2 (Supplementary Fig. 5D). We also demonstrated that overexpressing MCM2/5 reduced γ H2AX expression while increasing RAD51 expression in both A2780 and SKOV3 cell lines (Supplementary Fig. 5E). These findings provide functional evidence that MCM2/5 mediates acquired PARP inhibitor resistance in ovarian cancer cells, which is critical for understanding the resistance mechanism and developing therapeutic strategies to overcome it.

E2F1-Mediated Transcriptional Regulation of MCM2/5 Contributes to Niraparib Resistance in Ovarian Cancer

Having established the role of MCM2/5 in PARP inhibitor resistance, we investigated the transcriptional regulation of MCM2/5. The E2F family of transcription factors plays a crucial role in cell proliferation and regulation. In our previous study, E2F1 showed a significant upregulation trend among candidate genes in the niraparib-treated A2780R cell line (Supplementary Fig. 2A). Interrogation of the GEPIA database revealed a strong positive correlation between E2F1 and both MCM2 and MCM5 expression (Fig. 4B), supporting E2F1 as a potential transcriptional regulator. Further analysis in the JASPAR database identified four potential E2F1 binding sites in the promoters of MCM2 and MCM5 (Fig. 4C). Based on these sites, we designed specific primers and validated E2F1 binding to the MCM2 and MCM5 promoters using chromatin immunoprecipitation-polymerase

chain reaction (ChIP-PCR) experiments. The results showed that E2F1 antibodies significantly enriched MCM2 and MCM5 promoter sequences compared to negative control antibodies (Fig. 4D), supporting the hypothesis that E2F1 acts as a transcription factor for MCM2 and MCM5. Subsequent experiments demonstrated that E2F1 overexpression increased MCM2/5 mRNA and protein levels in A2780 cells (Fig. 4E, F), while silencing E2F1 with specific shRNA effectively reduced MCM2/5 RNA and protein levels in A2780R cells (Fig. 4G, H). To investigate whether E2F1 contributes to the acquired resistance to niraparib, we assessed the effect of E2F1 modulation on cell proliferation and drug sensitivity. Overexpressing E2F1 in parental A2780 cells significantly promoted cell proliferation and increased resistance to niraparib (Fig. 4I, K). In contrast, silencing E2F1 in A2780R cells restored sensitivity to niraparib and inhibited cell proliferation, as shown by cell viability assays (Fig. 4J, L). Collectively, these results reveal that E2F1 enhances MCM2/5 expression by directly binding to their promoters, leading to increased resistance to niraparib. This transcriptional regulation mechanism provides a compelling rationale for targeting the E2F1-MCM2/5 axis to overcome PARP inhibitor resistance in ovarian cancer.

CDK4/6-Mediated Modulation of the RB/E2F1-MCM2/5 Pathway Reverses Niraparib Resistance

Given the critical role of E2F1 in regulating MCM2/5 expression, and knowing that E2F1 is a downstream target of CDK4/6, which activates E2F1 by phosphorylating the RB (P-RB) protein and releasing its inhibition (Fig. 4A), we explored the potential of combining CDK4/6 inhibitors with PARP inhibitors to overcome PARP inhibitor resistance. In niraparib-resistant cell lines, CDK4/6, MCM2/5 and E2F1 are significantly upregulated (Fig. 2H, K). We assessed drug interactions using Synergy Finder 2.0, which indicated a favorable interaction between dalpiciclib (a CDK4/6 inhibitor) and niraparib at intermediate concentrations, with synergy scores of 12.701 in A2780R and 10.577 in SKOV3R cells (Fig. 5A), suggesting a synergistic effect between the two drugs in ovarian cancer. Compared to the IC₅₀ values of single-agent niraparib (38.01 μ M) and dalpiciclib (41.95 μ M) in A2780R cells, the IC₅₀ of the combination treatment (N + D) was significantly reduced to 12.58 μ M. Similar results were observed in SKOV3R cells (Fig. 5B). Compared to single drug treatments, the combination of dalpiciclib and niraparib significantly inhibited the proliferation and colony formation of drug-resistant ovarian cancer cells (Fig. 5C–E). Compared to single-drug treatments, the combination of dalpiciclib and niraparib significantly reduced the proportion of EdU-positive cells (Fig. 5F, G) and induced cell cycle arrest at the G2/M phase in drug-resistant ovarian cancer cells (Fig. 5H).

Mechanistically, the dalpiciclib-niraparib combination markedly disrupted the MCM2-MCM5 interaction (Fig. 5I). Furthermore, this combination treatment significantly reduced the expression of RB and P-RB, as well as the levels of E2F1 and RAD51, while increasing the level of the DNA damage marker γ H2AX (Fig. 5J). Similarly, the combination of fluzoparib and dalpiciclib significantly reduced the MCM2/5 interaction (Supplementary Fig. 3E) and correspondingly suppressed the expression of RB, P-RB, E2F1, and RAD51, while also increasing γ H2AX levels (Supplementary Fig. 3F). To further validate our findings, we profiled the mRNA levels of

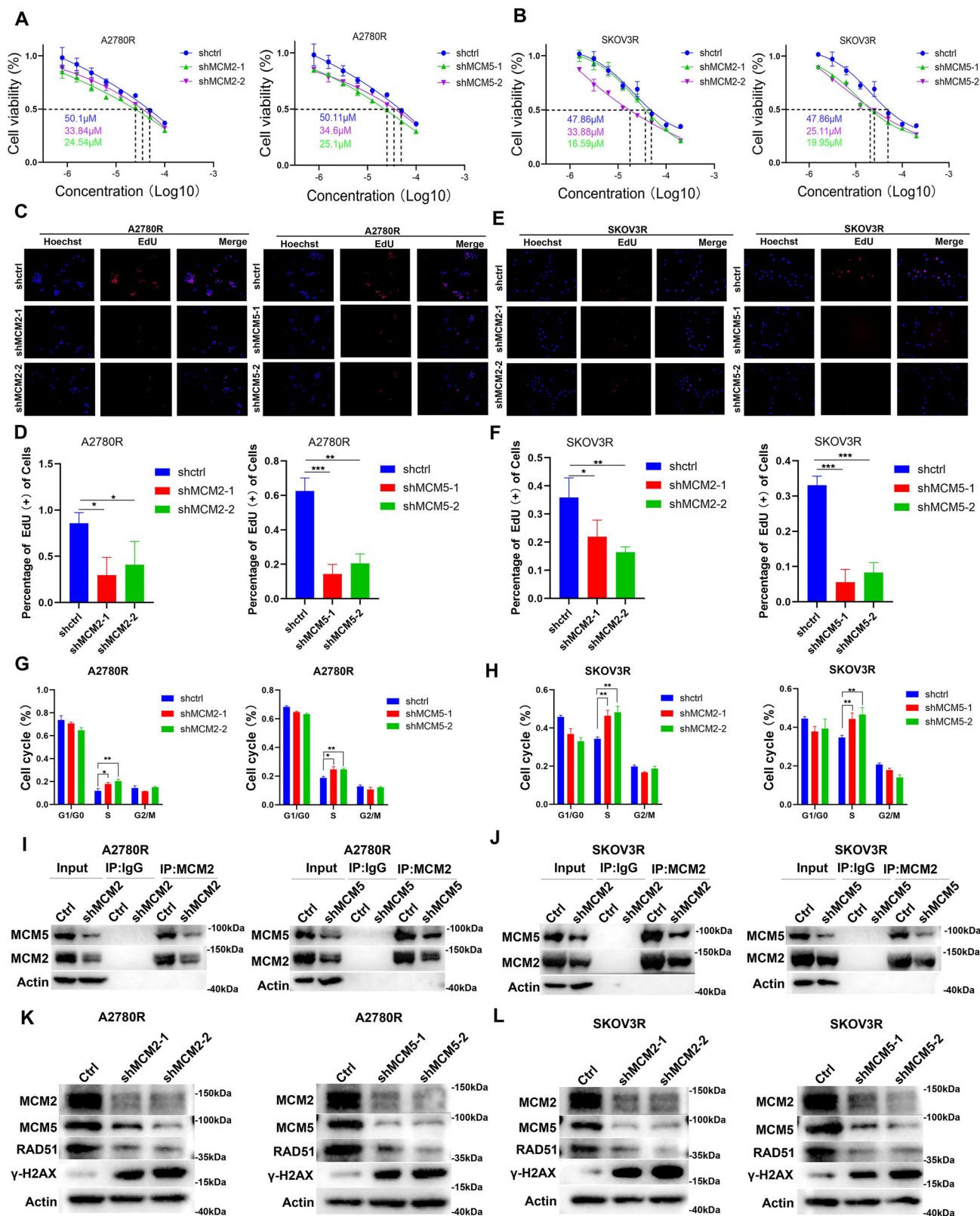


Fig. 3 | MCM2/5 knockdown restores sensitivity to niraparib in resistant ovarian cancer cells. A, B MCM2/5 knockdown in A2780R and SKOV3R cells repressed proliferation. **C, E** EdU assay shows that MCM2/5 knockdown in A2780R and SKOV3R cells repressed proliferation. **D, F** EdU formation of MCM2/5 knockdown in A2780R and SKOV3R cells repressed proliferation. **G, H** Cell cycle formation of

A2780R and SKOV3R cells after MCM2/5 knockdown. **I, J** Co-IP assay revealing the altered MCM2–MCM5 interaction in A2780R and SKOV3R cells after MCM2/5 knockdown. **K, L** The expressions of MCM2, MCM5, RAD51, and γH2AX were examined by Western blot in A2780R and SKOV3R cells after MCM2/5 knockdown. **P* < 0.05, ***P* < 0.01, ****P* < 0.001, *****P* < 0.0001.

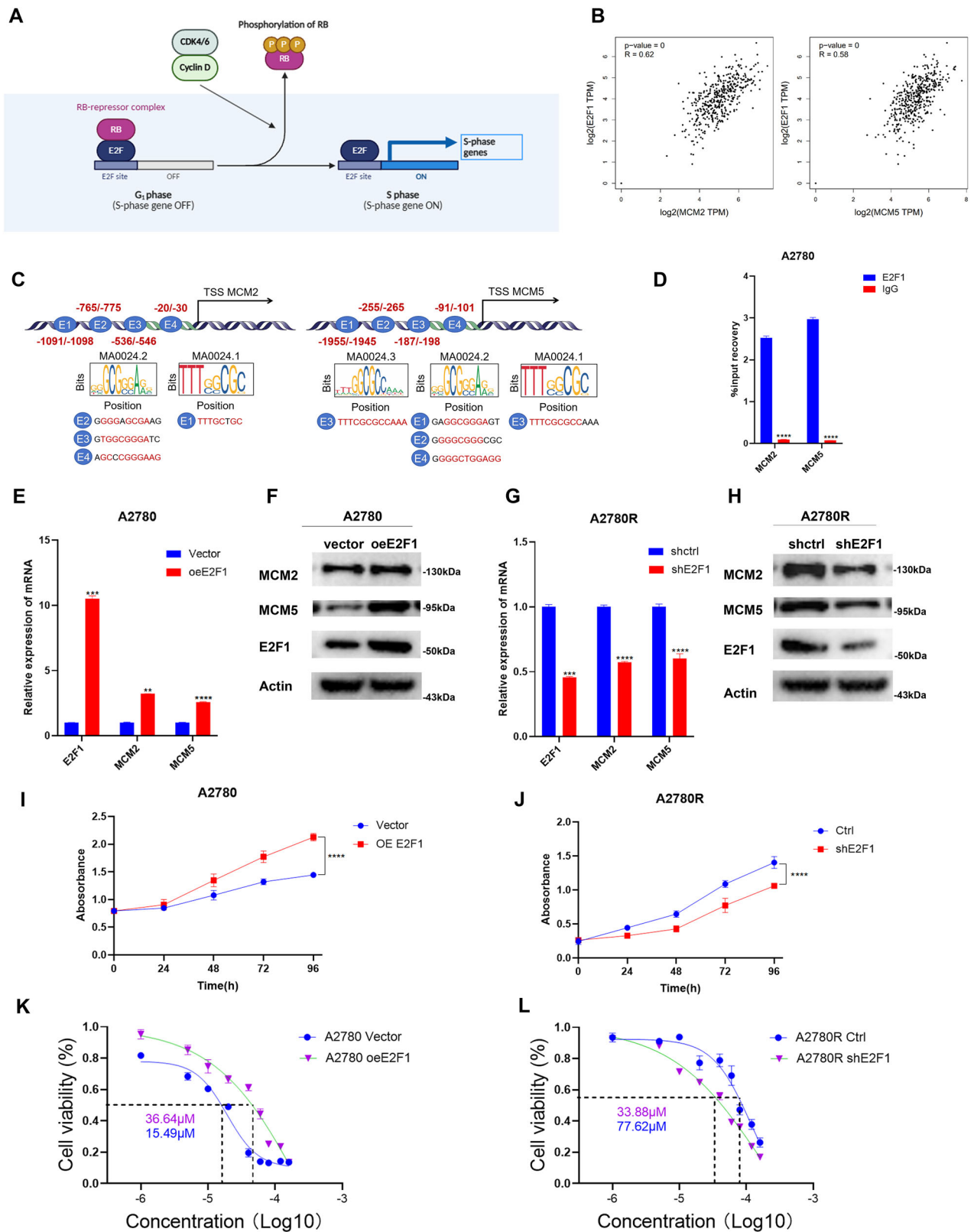
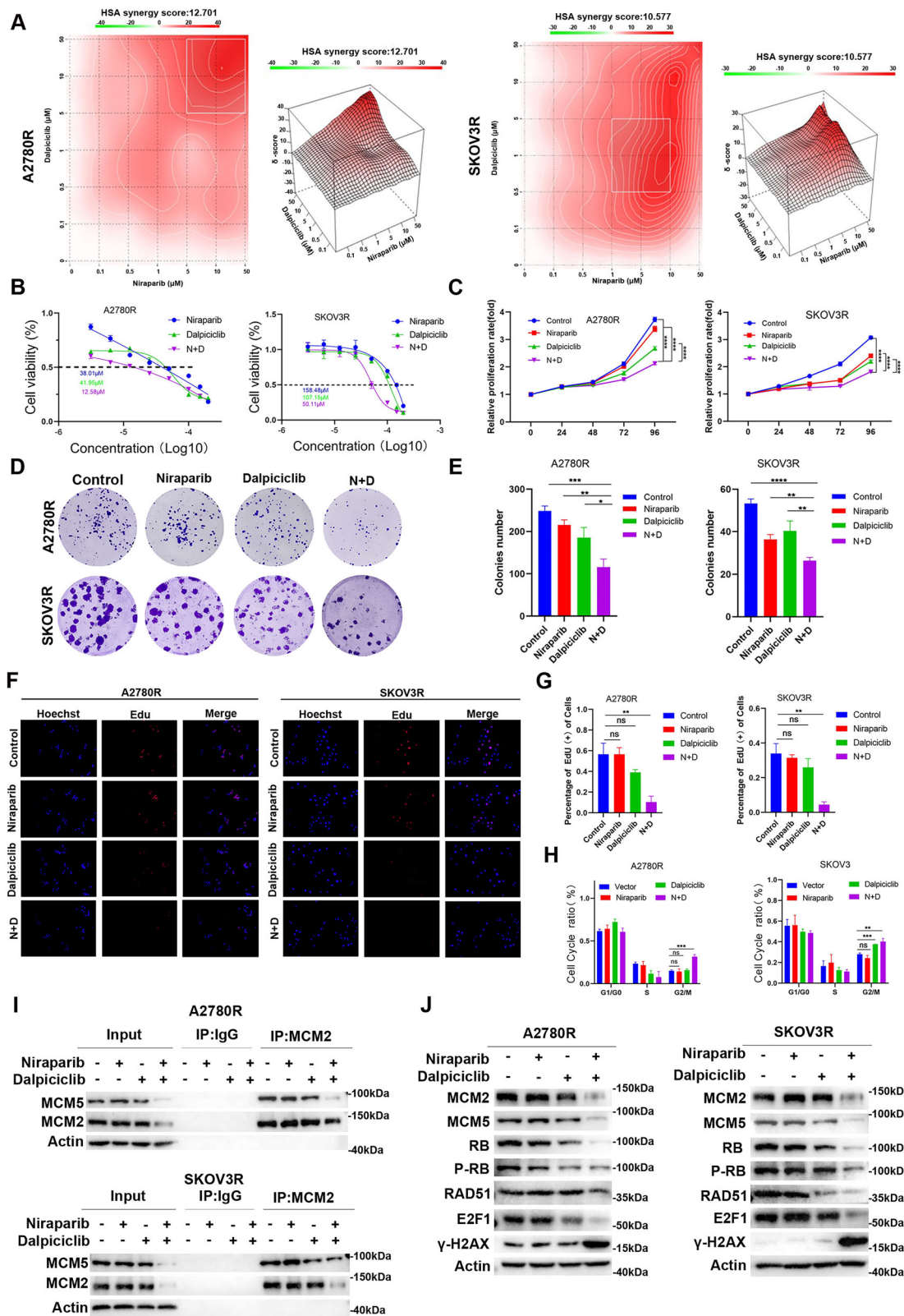


Fig. 4 | E2F1 binding to the MCM2/5 promoters and its effect on Niraparib resistance in ovarian cancer cells. **A** Schematic diagram of the RB/E2F pathway. **B** Scatter plots showing the correlation of MCM2/5 expression with E2F1 in OC cells based on the TCGA LIHC dataset. **C** Schematic illustration of putative E2F1-binding sites in the MCM2 and MCM5 promoter region. ChIP 1, 2, 3, and 4 indicate the predicted E2F1 binding sites. **D** Quantification of MCM2 and MCM5 promoters in ChIP-PCR using E2F1 antibody and IgG antibody in A2780 cells. **E, F** Overexpression of E2F1 and detection of expression levels of E2F1, MCM2, and

MCM5 by RT-PCR and Western Blot in A2780. **G, H** Knockdown of E2F1 and detection of expression levels of E2F1, MCM2, and MCM5 by RT-PCR and Western Blot in A2780R. **I, K** Overexpression of E2F1 in A2780 cells and subsequent treatment with niraparib to assess Drug-response curves of survival and IC50 values for cell viability by MTT assay. **J, L** Knockdown of E2F1 in A2780R cells and subsequent treatment with niraparib to assess Drug-response curves of survival and IC50 values for cell viability by MTT assay **P* < 0.05, ***P* < 0.01, ****P* < 0.001, *****P* < 0.0001.



E2F1-8 and MCM2/5 by RT-PCR in A2780R cells following treatment with abemaciclib, another CDK4/6 inhibitor. Notably, both dapiciclib and abemaciclib treatment led to consistent downregulation of E2F1 and MCM2/5 mRNA expression in A2780R cells (Supplementary Fig. 6A). Combination treatment with Niraparib and abemaciclib reduced the interaction between MCM2 and MCM5 (Supplementary Fig. 6B). We

further examined the protein expression levels of RB, P-RB, E2F1, MCM2/5, and γH2AX in A2780R cells treated with niraparib alone or in combination with abemaciclib. The combination of Niraparib and abemaciclib resulted in a decrease in the expression of RB, P-RB, E2F1, and MCM2/5, while also increasing the level of the DNA damage marker γH2AX (Supplementary Fig. 6C). Furthermore, the combination of Niraparib and dapiciclib led to a

Fig. 5 | Inhibition of CDK4/6 restores sensitivity to niraparib in resistant ovarian cancer cells by downregulating the RB/E2F1-MCM2/5 axis. **A** HSA synergy plots of dalpiciclib + niraparib in A2780R and SKOV3R cells. The synergy score was calculated using SynergyFinder2.0 software. Positive or negative HSA synergy scores indicated synergistic and antagonistic effects, respectively. **B, C** Drug-response curves of survival and IC50 values for cell viability after the treatment of a series of concentrations of niraparib, dalpiciclib and the combination of niraparib + dalpiciclib by MTT assays in A2780R and SKOV3R cells. **D, E** Colony formation assays after the treatment of a series of concentrations of niraparib, dalpiciclib, and the combination of niraparib + dalpiciclib in A2780R and SKOV3R cells. **F, G** Edu

formation after the treatment of a series of concentrations of niraparib, dalpiciclib, and the combination of niraparib + dalpiciclib in A2780R and SKOV3R cells. **H** Cell cycle formation after the treatment of a series of concentrations of niraparib, dalpiciclib, and the combination of niraparib + dalpiciclib in A2780R and SKOV3R cells. **I** Co-IP assay revealing the altered MCM2-MCM5 interaction in A2780R and SKOV3R cells between control, niraparib, dalpiciclib, and the combination of niraparib + dalpiciclib. **J** The expressions of MCM2, MCM5, RB, P-RB, RAD51, E2F1, and γ H2AX were examined by Western blot between control, niraparib, dalpiciclib, and the combination of niraparib + dalpiciclib in A2780R and SKOV3R. * $P < 0.05$, ** $P < 0.01$, *** $P < 0.001$, **** $P < 0.0001$.

significant increase in the sensitivity of the parental A2780 and SKOV3 cell lines to Niraparib (Supplementary Fig. 7A), and notably inhibited cell proliferation and clonogenic survival (Supplementary Figs. 7B-D). These findings suggest that CDK4/6 inhibitors target CDK4/6, leading to inhibition of RB/E2F1 signaling and reversal of niraparib resistance. This provides a rationale for combination therapies targeting the CDK4/6-RB-E2F1-MCM2/5 axis to overcome PARP inhibitor resistance.

Dalpiciclib and Niraparib Synergistically Suppress Niraparib-Resistant Tumor Growth In Vivo

To validate our in vitro findings and assess the clinical potential of the combination therapy, we established subcutaneous xenograft models in nude mice using both parental A2780 and A2780R cells (Fig. 6A). After a 7-day acclimatization period, the experimental procedures were initiated. Treatment commenced on day 21 and was administered orally via gavage. Mice were randomly divided into four groups (three mice per group) receiving vehicle control, niraparib 50 mg/kg, dalpiciclib 50 mg/kg, or a combination of niraparib and dalpiciclib. The treatment commenced on day 14 after tumor cell inoculation and was administered daily until day 42. In both parental A2780 and A2780R tumor models, the combination of niraparib and dalpiciclib significantly inhibited tumor growth, particularly in niraparib-resistant tumors, compared to the vehicle control group. Importantly, the combination therapy demonstrated a stronger tumor inhibitory effect than either drug alone (Fig. 6B-D, Supplementary Fig. 7E-G). Subsequently, we performed immunohistochemical (IHC) staining for Ki-67, MCM2/5, and E2F1 on serial sections of resected tumors. Compared to single drug treatments, the combination therapy significantly reduced the expression of Ki67, MCM2/5, and E2F1 (Fig. 6E, Supplementary Fig. 6H). These in vivo results corroborate our in vitro findings, demonstrating that the combination of dalpiciclib and niraparib can effectively inhibit the growth of niraparib-resistant tumors through downregulation of MCM2/5, providing compelling evidence for the clinical application of this combination therapy to overcome PARP inhibitor resistance in ovarian cancer. Figure 6F illustrates that tumor cell survival in Niraparib-resistant models is driven by the upregulation of MCM2/5 expression, enhanced DNA replication, reduced DNA damage, and increased RAD51 expression, promoting homologous recombination repair (HRR). The combination therapy of Niraparib and a CDK4/6 inhibitor targets this pathway by inhibiting the CDK4/6-RB-E2F1-MCM2/5 axis and HRR upregulation, ultimately leading to tumor cell death.

Discussion

New mechanisms of PARP inhibitor resistance are urgently needed to guide treatment strategies to overcome PARP inhibitor resistance in OC. The MCMs are the best-known proteins involved in the initiation of DNA replication and related to the sensitivity of chemotherapy and targeted drugs. However, whether MCMs are involved in PARP inhibitor resistance in OC has not been studied and reported yet.

In recent studies, it has been shown that the disruption of the MCM complex can lead to reduced DNA replication and cell-cycle progression in drug-resistant cancers. For example, Lin et al. reported that AS4583 inhibited cell-cycle progression and reduced DNA replication by disrupting the formation of the MCM complex to suppress drug-resistant non-small-cell lung cancer cells¹⁶. In small-cell lung cancer, knockdown of *MCM2*,

MCM4, *MCM6*, and *MCM7* genes showed significant attenuation of cancer cell proliferation and enhanced cisplatin sensitivity¹⁷. Inhibition of MCM2 enhanced the sensitivity of ovarian cancer cells to carboplatin¹⁸. Thiazobenzazole inhibited proliferation and invasion in human glioblastoma multiforme cells through targeting MCM2¹⁹. Long-term exposure to genistein reduced the tyrosine kinase activity of ERBB2 and impaired the function of the PTK6-AKT-GSK3 β axis, leading to downregulation of the MCM complex in gallbladder cancer cells²⁰. MCM2 enhanced the stemness of HCC cells by affecting the Hippo signaling pathway, while the downregulation of MCM2 inhibits resistance towards sorafenib²¹.

Our study demonstrates that MCM2 and MCM5 promote PARP inhibitor resistance in OC cells, making them potential therapeutic targets for overcoming this resistance. Using RNA-Seq analysis, we found that MCM2/5 were significantly downregulated after PARP inhibitor (niraparib) treatment in parental OC cells and upregulated in NirR cell lines. Upregulated MCM2/5 mediated PARP inhibitor resistance, and MCM2/5 downregulation rescued sensitivity to PARP inhibitor in OC. MCM2/5 downregulation inhibited proliferation and reduced the proportion of cells in S-phase in NirR cells. MCM2-7 form a conserved set and promote DNA synthesis throughout S-phase²². A gap between MCM2 and MCM5 serves as a DNA entry gate in the MCM2-7 complex, which is crucial for DNA synthesis²³. Once the MCM complex is disrupted, cells undergo limited replication and are hypersensitive to the stresses of DNA replication, resulting in DNA damage and suppressing cell growth. This could explain why the loss of MCM2/5 function in PARP inhibitor-resistant OC cells during the S phase could generate chromosome instability and DNA damage, which further results in PARP inhibitor-resistant OC cells apoptosis increase and cell growth suppression in our data. This finding is supported by our experimental data, which show that both MCM2 and MCM5 were upregulated in the resistant cells, and their protein-protein interaction was significantly enhanced, as demonstrated by Co-IP. These results suggested that MCM2 and MCM5 may rely on a complex to play their roles in promoting OC progression.

Our data indicated that the combination of the CDK4/6 inhibitor (dalpiciclib) and PARP inhibitor (niraparib) showed anti-tumor activity and reversed PARP inhibitor resistance in vitro and in vivo via downregulating MCM2/5 in OC cells. Mechanistically, the combination downregulated MCM2/5 expression, disrupted the MCM2-MCM5 interaction, and concomitantly reduced the protein levels of E2F1, RB, and RAD51, while also increasing the level of γ H2AX. MCM2/5 may serve as potential targets for the combination therapy of CDK4/6 inhibitors and PARP inhibitors to overcome PARP inhibitor resistance. Accumulating evidence indicates that CDK4/6 plays a central and originally unanticipated role in the regulation of the DNA Damage Response (DDR), which suggests that CDK4/6 inhibitors may well cooperate with DNA or mitotic damaging agents to enhance their anti-tumor activity²⁴. Beyond inhibiting tumor cell proliferation, CDK4/6 inhibitors affect tumor cells and the tumor environment through mechanisms that are only beginning to be elucidated²⁵. Slamon and colleagues tried to identify which ovarian cancer types may be sensitive to CDK4/6 inhibitors²⁶. Yi et al. demonstrated therapeutic synergy for combined PARP and CDK4/6 inhibition and identified MYC status as a determinant of sensitivity in ovarian cancer cells²⁷. Tian et al. reported that a novel CDK4/6 and PARP dual inhibitor, ZC-22, effectively suppresses

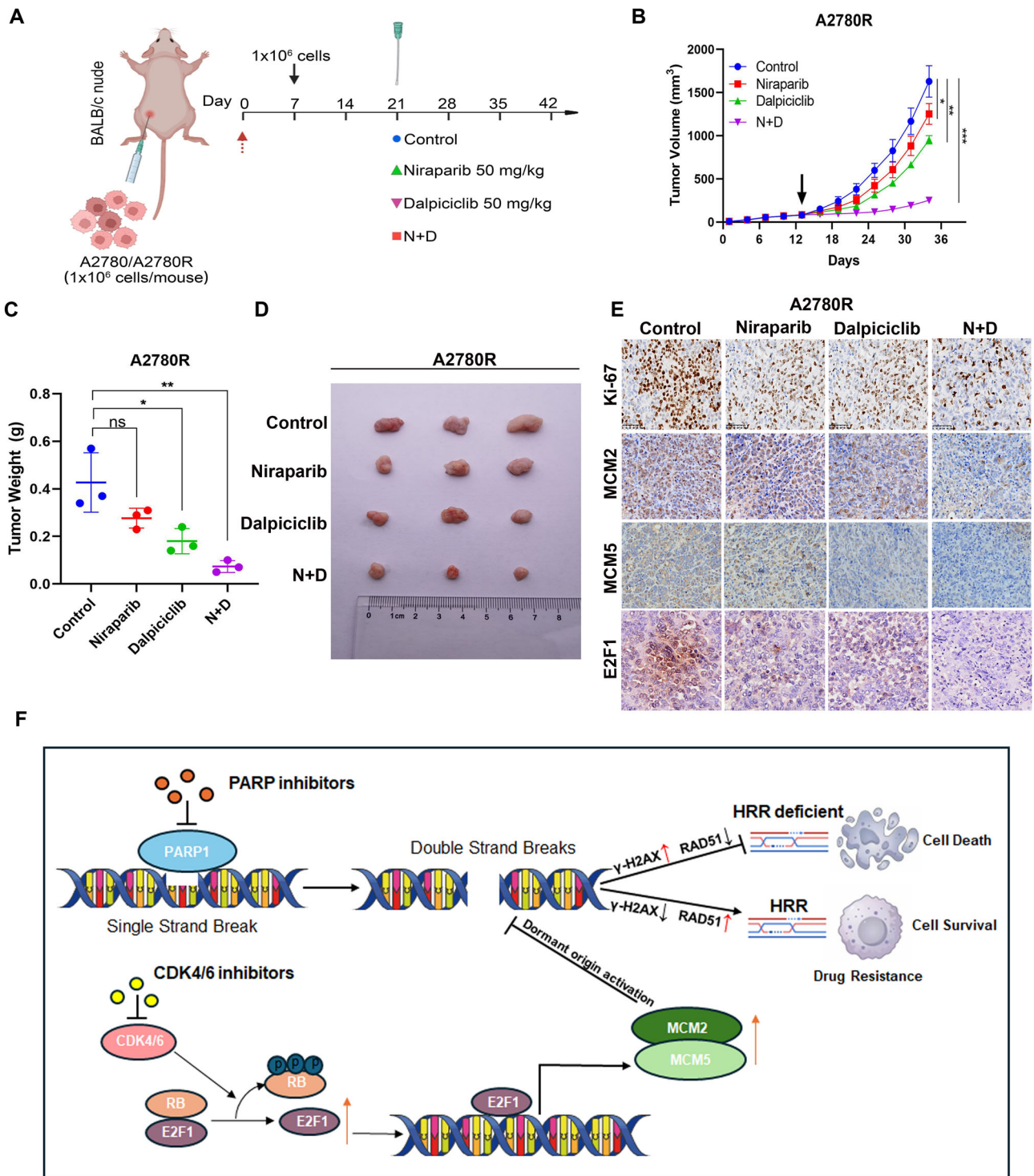


Fig. 6 | In vivo combination therapy with dalpiciclib and niraparib significantly inhibits the growth of Niraparib-resistant ovarian tumors. **A** Flow diagram of the in vivo experiments. **B** Tumor volume. **C** Tumor weight. **D** Images of tumors formed by A2780R cells in the indicated treatment groups. **E** Serial sections of A2780R tumors from the indicated treatment groups were subjected to

immunohistochemical staining using antibodies against Ki-67, MCM2, MCM5, and E2F1. **F** The combination therapy of Niraparib and a CDK4/6 inhibitor targets this pathway, inhibiting the CDK4/6-RB-E2F1-MCM2/5 axis and HRR upregulation, ultimately resulting in tumor cell death. * $P < 0.05$, ** $P < 0.01$, *** $P < 0.001$, **** $P < 0.0001$.

tumor growth and improves the response to cisplatin treatment in breast and ovarian cancer²⁸. Our work provides a novel mechanistic perspective on overcoming PARPi resistance by combining it with CDK4/6 inhibition. The prior study by Yi et al. identified MYC status as a critical factor. In contrast, we reveal a divergent pathway centered on the MCM2/5. We provide direct experimental evidence demonstrating an enhanced interaction between

MCM2 and MCM5 in resistant cells. We establish that CDK4/6 inhibition effectively targets this vulnerability by suppressing the E2F1-MCM2/5 axis and disrupting this strengthened interaction.

Previous studies reported that CDK4/6 plays a pivotal role in the transition from the G1 to S phases by regulating the phosphorylation state of the retinoblastoma-associated protein (RB). CDK4/6 also play a central role in

DNA replication and repair pathways by regulating the RB/E2F1 axis and thus are essential for cell-cycle progression in many cancer cells. In our data, the CDK4/6 inhibitor reversed PARP inhibitor resistance via downregulating MCM2/5 in PARPi-resistant OC cells. In canine cutaneous melanocytoma, cutaneous melanoma, oral melanoma, cervical cancer, and acute lymphoblastic leukemia (ALL), MCM2 is a target gene of E2F1. Our data also indicated that the CDK4/6 inhibitor can block the RB/E2F1 pathway and further downregulate E2F-mediated transcription, especially suppressing the target genes of E2F1-MCM2/5, thereby reversing PARP inhibitor resistance. Given the important roles of MCM2/5 in PARP inhibitor resistance, developing MCM2/5 inhibitors has important clinical prospects.

Our data represent the first report showing that the potential of inhibiting MCM2/5 to overcome PARPi resistance. The combination of the CDK4/6i and PARPi showed anti-tumor activity and reversed PARPi resistance in vitro and in vivo via downregulating MCM2/5 in OC cells. CDK4/6i reverse PARPi resistance by targeting the CDK4/6-RB-E2F1-MCM2/5 pathway. These results demonstrate the therapeutic potential of combining PARPi and CDK4/6 inhibition in treating patients with PARPi resistance in OC.

Methods

Cell Culture and Reagents

A2780, SKOV3, and 293 T cell lines were obtained from the Cell Bank of the Chinese Academy of Sciences (Shanghai, China). Cells were cultured in Dulbecco's Modified Eagle Medium (for A2780 cells) or McCoy's 5 A Medium (for SKOV3 cells), supplemented with 10% fetal bovine serum and penicillin/streptomycin (100 units/ml) at 37 °C in a 5% CO₂ incubator. Dalpiciclib and fluzoparib were generously provided by Hengrui Medicine Co. Ltd. (Jiangsu, China), while niraparib and abemaciclib were purchased from Selleck. Niraparib, dalpiciclib, and abemaciclib were dissolved in DMSO and further diluted in RPMI medium for experimental use. Antibodies used in this study included: mouse monoclonal anti-actin (#a3854), rabbit polyclonal anti-MCM2 (#10513-1-AP), rabbit polyclonal anti-MCM5 (#11703-1-AP), mouse monoclonal anti-MCM2 (#66204-1-Ig), rabbit polyclonal anti-MCM3 (#15597-1-AP), mouse monoclonal anti-MCM4 (#67103-1-Ig), mouse monoclonal anti-MCM5 (#67049-1-Ig), mouse monoclonal anti-MCM6 (#67989-1-Ig), rabbit polyclonal anti-MCM7 (#11225-1-AP), mouse monoclonal anti-E2F1 (#66515-1-Ig), rabbit polyclonal anti-RB1 (#10048-2-Ig), rabbit polyclonal anti-CDK4 (#11026-1-AP), rabbit polyclonal anti-CDK6 (#14052-1-AP), rabbit polyclonal anti-Phospho-RB1 (Ser807/811) (#30376-1-AP), rabbit polyclonal anti-RAD51 (#14961-1-AP), and rabbit polyclonal anti-Phospho-Histone H2A.X (Ser139) (#83307-2-RR). For monotherapy, cells were treated for 48 hours with the following concentrations: niraparib (A2780: 10 μM; A2780R: 30 μM; SKOV3: 30 μM; SKOV3R: 80 μM), fluzoparib (A2780: 10 μM; A2780R: 30 μM), dalpiciclib (A2780: 10 μM), and abemaciclib (A2780: 10 μM). For combination therapy, A2780R cells were treated with: niraparib (15 μM) plus dalpiciclib (5 μM); fluzoparib (15 μM) plus dalpiciclib (5 μM); or niraparib (15 μM) plus abemaciclib (5 μM). SKOV3R cells were treated with niraparib (40 μM) plus dalpiciclib (5 μM).

Generation of PARP inhibitor-resistant cells

To generate PARP inhibitor-resistant cells, A2780 and SKOV3 were subjected to gradual increases in niraparib concentrations until cells grew in the presence of niraparib (10 μM) from initial exposure. Then, PARP inhibitor-resistant cell lines (A2780R and SKOV3R) were developed by long-term drug exposure (>6 months; 10–300 μM of PARP inhibitor). To maintain the resistant phenotype, the resistant cells were cultured in low concentrations of niraparib (typically 1/10 of the IC₅₀ of the resistant cell lines). The resistance index is calculated as the ratio of the IC₅₀ of the resistant cell line to the IC₅₀ of the parental cell line.

RNA Sequencing Assay

A2780 and A2780R cells were exposed to Niraparib at concentrations of 10 μM and 30 μM for 48 h. Total RNA was then isolated and subjected to

RNA sequencing by BGI. RNA-sequencing assay included the cDNA library construction, library purification, and transcriptome sequencing. All experiments were carried out according to the protocols of the Wuhan Huada Sequencing Company. Three samples were used for each group of RNA-sequencing assay.

GO and KEGG Enrichment Analysis

GO and KEGG enrichment analyses revealed the functional roles of differentially expressed genes (DEGs). GO database was first used to analyze the functional enrichment of DEGs in terms of cellular components, molecular function, and biological process. The enrichment of DEGs was determined by the KEGG pathway database. The threshold was 0.05 to test the hypergeometric distribution of default enrichment results.

Quantitative Real-Time PCR

Cells were treated with the drug after 48 h. The total RNA of cells was extracted with Trizol reagent. FastKing RT kit was used to reverse-transcribe RNA to cDNA. qRT-PCR was performed with GoTaq[®] qPCR Master Mix. The glyceraldehyde-3-phosphate dehydrogenase (GAPDH) value was used as the normalized expression control. All the primers are shown in Table S1.

Western Blot Assay

Cells were treated with the drug after 48 h. Proteins were obtained from cell lysates with RIPA buffer. Bicinchoninic acid (BCA) assay kit was used to determine the concentration of protein. The total lysates were subjected to sodium dodecyl sulfate (SDS)-loading buffer at 100 °C and then exposed to sodium dodecyl sulfate polyacrylamide gel electrophoresis (SDS-PAGE). Polyvinylidene difluoride (PVDF) membranes were transferred with protein and blocked with 5% dried skimmed milk. Specific primary antibodies were incubated with PVDF membranes overnight. Then, HRP-conjugated secondary antibody was added, and the expression of the protein was examined with the ECL plus reagents.

Cell proliferation, colony formation, cell cycle analysis

Cells were seeded and treated with the indicated doses of niraparib, dalpiciclib, or both. Cell survival and colony formation ability assays were performed to evaluate the efficacy of niraparib and dalpiciclib at indicated doses by MTT (at 5 days) and crystal violet staining (at 10 days), respectively. We performed the EdU assay according to the instructions of the Cell-Light[™] EdU Apollo[®] In Vitro Kit (C10310-1). For cell cycle detection, cells were incubated with drugs (48 h) and then labeled with propidium iodide (PI) solution and analyzed by flow cytometry (Beckman CytoFlex). Data were analyzed by FlowJo software (Tree Star, Inc., Ashland, OR).

Plasmids and transfection

A2780R and SKOV3R cells were transfected with pLKO.1-MCM2/5 or an empty plasmid, and A2780 and SKOV3 cells were transfected with PLVX 3xFLAG-MCM2/5 or an empty plasmid using Hieff Trans[™] Liposomal Transfection Reagent (Yeasen Biotechnology Co. Ltd.), according to the manufacturer's instructions. The sequences of shRNA used in knockdown experiments are provided in Table S1.

Chromatin immunoprecipitation assay

Chromatin immunoprecipitation (ChIP) assays were performed using the ChIP Assay kit (#P2078). Cells were cross-linked with 1% formaldehyde for 10 min at 37 °C and quenched in glycine. DNA was immunoprecipitated from the sonicated cell lysates using the E2F1 antibody (#66515-1-Ig) and subjected to PCR to amplify the E2F1-binding sites. Chromatin (10%) was used before immunoprecipitation as the input control, and a nonspecific antibody against IgG served as the negative control.

Calculation of Drug Combination Index

The drug combination effects were assessed in A2780R and SKOV3R cell lines using a 7 × 7 dose-response matrix for the two drugs. The resulting data

were analyzed with the HAS model to calculate a synergy score. According to this model, a synergy score between -10 and 0 indicates antagonism, a score between 0 and 10 suggests an additive effect, and a score greater than 10 demonstrates synergy. The analysis of drug interaction and calculation of synergy scores were performed using the SynergyFinder web tool (version 2.0; <https://synergyfinder.fimm.fi>).

Histological and Immunohistochemical Staining Analysis

Tumors were fixed in 10% buffered formalin overnight before paraffin embedding. Paraffin blocks were sectioned and stained with haematoxylin and eosin (H&E). The value for tumor cell density was calculated as the number of tumor cells per mm². For immunohistochemical staining analysis, rabbit polyclonal anti-MCM2 (#10513-1-AP), rabbit polyclonal anti-MCM5 (#11703-1-AP), mouse monoclonal anti-Ki67(#P46013), and mouse monoclonal anti-E2F1 (#66515-1-Ig) were used.

Tumor Model of Animal Experiments

The Animal Care and Use Committee of Xiamen University conducted the following protocols for all animal experiments. 120 μ l A2780/A2780R cell suspension with concentration of 3×10^6 /ml was injected subcutaneously into right dorsal flank of BALB/c nude mice (6-week-old female). The drug treatment started when the tumor xenografts reached approximately 75 mm³. Niraparib and dalpiciclib were dissolved in 0.5% CMC-Na solution and administered via oral gavage at 50 mg/kg/day. Tumors were measured every other day with digital calipers and calculated using the following formula: tumor volume = (length \times width²)/2. At the experimental endpoint (tumor volume \approx 1500 mm³ or 3-week post-treatment), mice were deeply anesthetized by intraperitoneal injection of pentobarbital sodium (100 mg kg⁻¹) and sacrificed by cervical dislocation while still unconscious. This dose produces rapid loss of consciousness within \leq 30 s and ensures no recovery, minimizing animal suffering. The method was approved by the Animal Care and Use Committee of Xiamen University (protocol XMU-LAC20220195) and is consistent with the AVMA Guidelines for the Euthanasia of Animals.

Statistical analysis

PFS was estimated by the Kaplan-Meier method with log-rank analysis. Gene expression and gene expression correlations were retrieved from the GEPIA database. Transcription factor binding site prediction was performed using the JASPAR database, which was utilized to identify potential binding sites for candidate transcription factors in the promoters of MCM2 and MCM5. MTT, colony formation assays, flow cytometry, and western blots were performed using at least three biological replicates per sample and as three independent experiments. Unpaired Student's t-test and one-way ANOVA with Tukey's multiple-comparisons tests were performed using GraphPad Prism 9 software for analysis of the data obtained in vitro and in vivo, respectively. $P < 0.05$ was considered statistically significant.

Data availability

All data supporting the findings of this study are available within the article and its supplementary file. The raw RNA-seq data reported in this paper have been deposited in the NCBI Sequence Read Archive (SRA) under accession number PRJNA1380441. The data can be obtained immediately by contacting the corresponding author with a brief project description.

Received: 25 August 2025; Accepted: 20 February 2026;

Published online: 07 March 2026

References

- Konstantinopoulos, P. A. & Matulonis, U. A. Clinical and translational advances in ovarian cancer therapy. *Nat. Cancer* **4**, 1239–1257 (2023).
- McMellen, A. et al. ATF6-Mediated Signaling Contributes to PARP Inhibitor Resistance in Ovarian Cancer. *Mol. Cancer Res.* **21**, 3–13 (2023).
- Bednarikova, M. et al. Can Schlafen 11 Help to Stratify Ovarian Cancer Patients Treated with DNA-Damaging Agents? *Cancers (Basel)* **14**, 2353 (2022).
- Zhang, X. et al. Targeting polyploid giant cancer cells potentiates a therapeutic response and overcomes resistance to PARP inhibitors in ovarian cancer. *Sci. Adv.* **9**, eadf7195 (2023).
- Miller, R. E., El-Shakankery, K. H. & Lee, J. Y. Lee, PARP inhibitors in ovarian cancer: overcoming resistance with combination strategies. *J. Gynecol. Oncol.* **33**, e44 (2022).
- Cordani, N. et al. An Overview of PARP Resistance in Ovarian Cancer from a Molecular and Clinical Perspective. *Int. J. Mol. Sci.* **24**, 11890 (2023).
- Wang, Y. et al. MCM family in gastrointestinal cancer and other malignancies: From functional characterization to clinical implication. *Biochim Biophys. Acta Rev. Cancer* **1874**, 188415 (2020).
- Zhang, X. et al. Minichromosome maintenance protein family member 6 mediates hepatocellular carcinoma progression by recruiting UBE3A to induce P53 ubiquitination. *Int J. Biol. Macromol.* **248**, 125854 (2023).
- Yu, S. et al. MCMs in Cancer: Prognostic Potential and Mechanisms. *Anal. Cell Pathol. (Amst.)* **2020**, 3750294 (2020).
- Liu, Z. et al. MCM family in HCC: MCM6 indicates adverse tumor features and poor outcomes and promotes S/G2 cell cycle progression. *BMC Cancer* **18**, 200 (2018).
- Yang, X. et al. Minichromosome maintenance gene family: potential therapeutic targets and prognostic biomarkers for lung squamous cell carcinoma. *Aging (Albany NY)* **14**, 9167–9185 (2022).
- Wu, B. & Xi, S. Bioinformatics analysis of the transcriptional expression of minichromosome maintenance proteins as potential indicators of survival in patients with cervical cancer. *BMC Cancer* **21**, 928 (2021).
- Saito, Y. et al. MCMBP promotes the assembly of the MCM2-7 hetero-hexamers to ensure robust DNA replication in human cells. *Elife.* **11**, e77393 (2022).
- Sun, Y. et al. MCM2 in human cancer: functions, mechanisms, and clinical significance. *Mol. Med* **28**, 128 (2022).
- Bailis, J. M. et al. MCM proteins: DNA damage, mutagenesis and repair. *Curr. Opin. Genet. Dev.* **14**, 17–21 (2004).
- Lin, C. Y. et al. Suppression of Drug-Resistant Non-Small-Cell Lung Cancer with Inhibitors Targeting Minichromosomal Maintenance Protein. *J. Med. Chem.* **63**, 3172–3187 (2020).
- Misono, S. et al. Molecular Signature of Small Cell Lung Cancer after Treatment Failure: The MCM Complex as Therapeutic Target. *Cancers (Basel)* **13**, 1187 (2021).
- Deng, M. et al. Inhibition of MCM2 enhances the sensitivity of ovarian cancer cell to carboplatin. *Mol. Med Rep.* **20**, 2258–2266 (2019).
- Hu, Y. et al. Thiabendazole Inhibits Glioblastoma Cell Proliferation and Invasion Targeting Mini-chromosome Maintenance Protein 2. *J. Pharm. Exp. Ther.* **380**, 63–75 (2022).
- Geng, Y. et al. Long-term exposure to genistein inhibits the proliferation of gallbladder cancer by downregulating the MCM complex. *Sci. Bull. (Beijing)* **67**, 813–824 (2022).
- Zhou, X. et al. MCM2 promotes the stemness and sorafenib resistance of hepatocellular carcinoma cells via Hippo signaling. *Cell Death Discov.* **8**, 418 (2022).
- Ticau, S. et al. Mechanism and timing of Mcm2-7 ring closure during DNA replication origin licensing. *Nat. Struct. Mol. Biol.* **24**, 309–315 (2017).
- Zhai, Y. et al. Open-ringed structure of the Cdt1-Mcm2-7 complex as a precursor of the MCM double hexamer. *Nat. Struct. Mol. Biol.* **24**, 300–308 (2017).
- Goel, S., Bergholz, J. S. & Zhao, J. J. Targeting CDK4 and CDK6 in cancer. *Nat. Rev. Cancer* **22**, 356–372 (2022).
- Fassl, A., Geng, Y. & Sicinski, P. CDK4 and CDK6 kinases: From basic science to cancer therapy. *Science* **375**, eabc1495 (2022).

26. Dall'Acqua, A. et al. Inhibition of CDK4/6 as Therapeutic Approach for Ovarian Cancer Patients: Current Evidences and Future Perspectives. *Cancers (Basel)*. **13**, 3035 (2021).
27. Yi, J. et al. MYC status as a determinant of synergistic response to Olaparib and Palbociclib in ovarian cancer. *EBioMed*. **43**, 225–237 (2019).
28. Tian, C. et al. A Novel CDK4/6 and PARP Dual Inhibitor ZC-22 Effectively Suppresses Tumor Growth and Improves the Response to Cisplatin Treatment in Breast and Ovarian Cancer. *Int. J. Mol. Sci.* **23**, 2892 (2022).

Acknowledgements

This work was supported by Shenzhen Science and Technology Program (JCYJ20210324121802008, JCYJ20220530143406015), Medical Innovation Project of Fujian Provincial Health Commission (2023CXB006), Xiamen Natural Science Foundation Project (3502Z20227266), the Natural Science Foundation of Fujian Province (20247011335), the Open Research Project of the Key Laboratory of Prevention and Treatment of Cardiovascular and Cerebrovascular Diseases (Ministry of Education), Gannan Medical University (XN202005) and the Scientific Research Foundation of State Key Laboratory of Vaccines for Infectious Diseases, Xiang An Biomedicine Laboratory (2023XAKJ0101005). We also thank Hengrui Medicine Co. Ltd. (Jiangsu, China) for its help in providing dalpiciclib and fluzoparib.

Author contributions

L.X. and T.H. conceived and supervised the study. Y.F., M.F., and B.Z. performed data curation. F.L., X.H., Q.C., and W.T. conducted investigation and formal analysis. K.R., X.H., and H.S. developed the methodology. W.Z., F.L., L.X., and H.S. provided resources. F.L., X.H., B.Z., M.F., and Y.F. conducted software and validation analysis. B.Z. and Y.F. were responsible for visualization. Y.F., M.F., B.Z., and F.L., L.X. and T.H. wrote the original draft. L.X., T.H., and H.S. reviewed and edited the manuscript. All authors read and approved the final version.

Competing interests

The authors declare no competing interests.

Additional information

Supplementary information The online version contains supplementary material available at <https://doi.org/10.1038/s41698-026-01353-w>.

Correspondence and requests for materials should be addressed to Huibo Shi, Tianhui Hu or Li Xiao.

Reprints and permissions information is available at <http://www.nature.com/reprints>

Publisher's note Springer Nature remains neutral with regard to jurisdictional claims in published maps and institutional affiliations.

Open Access This article is licensed under a Creative Commons Attribution-NonCommercial-NoDerivatives 4.0 International License, which permits any non-commercial use, sharing, distribution and reproduction in any medium or format, as long as you give appropriate credit to the original author(s) and the source, provide a link to the Creative Commons licence, and indicate if you modified the licensed material. You do not have permission under this licence to share adapted material derived from this article or parts of it. The images or other third party material in this article are included in the article's Creative Commons licence, unless indicated otherwise in a credit line to the material. If material is not included in the article's Creative Commons licence and your intended use is not permitted by statutory regulation or exceeds the permitted use, you will need to obtain permission directly from the copyright holder. To view a copy of this licence, visit <http://creativecommons.org/licenses/by-nc-nd/4.0/>.

© The Author(s) 2026